BOUNDARY CONDITIONS FOR 3-D DYNAMIC MODELS OF ABLATION OF CERAMICS BY PULSED MID-INFRARED LASERS

A. Vila Verde, Marta M. D. Ramos[*]

Department of Physics, University of Minho, Campus de Gualtar, 4710-057 BRAGA,

PORTUGAL

_____

Abstract

We present and discuss a set of boundary conditions (BCs) to use in 3-dimensional, mesoscopic, finite element models of mid-infrared pulsed laser ablation of brittle materials. These models allow the study of the transient displacement and stress fields generated at micrometer scales during and after one laser pulse, where using conventional BCs may lead to some results without physical significance that can be considered an artefact of the calculations. The proposed BCs are tested and applied to a micrometer-scale continuous model of human dental enamel under CO_2 radiation (10.6 µm, 0.35 µs pulse, sub-ablative

[*] Corresponding Author: Tel. +351 253 604 330; Fax. +351 253 678 981; E-mail: marta@fisica.uminho.pt

fluence), giving rise to the following results: the highest stress is obtained at the irradiated surface of the model, at the end of the laser pulse, but afterwards it decreases rapidly until it becomes significantly lower than the stress in a region 2.5 µm deep in the model; a thermally-induced vibration in the material is predicted. This non-intuitive dynamics in stress- and displacement-distribution cannot be neglected and has to be considered in dynamic laser ablation models, since it may have serious implications in the mechanisms of ablation.

keywords: mesoscopic modelling; laser ablation; enamel; finite elements; infrared laser; boundary conditions.

Departamento de Física, Universidade do Minho, Campus de Gualtar, 4710-057 BRAGA, PORTUGAL

1. Introduction

The ablation of ceramic materials using pulsed mid-infrared (IR) lasers has been used in industrial, research and medical environments for several years now. Despite the large amount of work which has been done with the aim of understanding the mechanisms of ablation, high level comprehension of these mechanisms does not exist yet, and neither do models with sufficient predictive ability to contribute to the optimization of existing procedures.

Our group is developing general, dynamic 3-dimensional finite element (FE) models to understand the ablation mechanisms of ceramic composite materials by pulsed mid-infrared lasers. These models include the structure of the material at mesoscopic scales, known to play an important role during ablation [1,2]. Therefore, the models represent micrometer-size pieces of the macroscopic object under laser radiation. In general, theoretical calculations contain the assumption that, for sufficiently large models, the bulk properties will be reproduced. However, the model properties approach the bulk ones rather slowly and they are not monotonic functions of model size. While the use of large models is conceptually desirable, it becomes computationally prohibitive. Therefore, one needs to use smaller models to attempt, at some level of approximation, to reproduce the properties for the entire system. This led us to the important problem of determining which boundary conditions (BCs) should be applied to the FE models so that one could effectively simulate a piece of material which is a part of a larger object. Appropriate BCs are determinant to obtain meaningful results; however, this problem has not been specifically addressed in the literature, to the best of our knowledge; authors doing computational and theoretical research on ablation either choose periodic BCs for their models, or assume an infinite or semi-infinite material [3,4]. Their models provided an important starting point for the elucidation of ablation mechanisms, but further work on the subject still needs to be done to fully understand the physics underlying laser ablation at mesoscopic scales. Developing easy-to-apply BCs for dynamic FE models

2

that adequately account for the finite size and constraints of the region of material being simulated, at the micrometer scale, is the purpose of this work. We have already done this in the context of our static stress FE models applied to the study of human dental enamel ablation [5,6]. Faced with the more complicated problem of applying BCs to a model intended to capture the dynamic processes taking place during ablation, we built on the general approach followed on the static model and developed a new set of BCs appropriate for dynamic models, which are presented and discussed in this paper.

2. Model description

We are using ABAQUS 6.3 and 6.4 (commercial Finite Element software) to develop laser ablation models. Despite the large amount of experimental and theoretical work already done, the ablation of human dental enamel by pulsed CO_2 lasers - a procedure of growing importance in dentistry - is not yet optimised (the ablation rates are lower than what is clinically desirable, and unwanted side effects such as cracking or over-heating of tissue may occur when higher fluences or repetition rates are used). This makes it an ideal system to address modelling questions such as BCs that should also be applied to ablation models of other ceramic materials by mid IR lasers.

The temperature field generated in enamel by absorption of radiation induces a stress field but, since the mechanical energy-dissipation processes in such a brittle material are normally not associated with plastic straining, the stress field does not generate heat. Therefore, the appropriate way to model the response of enamel to laser radiation of sub-ablative intensity is to use sequential thermal stress analyses: first only the thermal problem is modelled (using transient heat transfer analysis) and the temperature field during and after one laser pulse is obtained. This temperature field then serves as input to the dynamic stress

analysis. Given the short duration of the laser pulse, it is reasonable to use the dynamic explicit algorithm for the stress analysis.

The laser beam was considered perpendicular to the top and bottom surfaces of the model. The intensity of the beam inside the tissue is given by

$$I(r,z) = I_0 \exp(-\mu z).\exp(-2r^2/w^2),\tag{1}$$

where z is the depth inside the tissue, I_0 is the intensity of radiation at the surface of the target, μ is the absorption coefficient of the tissue, w is the beam radius and r is the radial distance from the centre of the laser spot [7]. The heat deposited per unit area and time, S(r,z), over a slice of material of thickness dz is given by

$$S(r,z) = -\frac{\partial I(r,z)}{\partial z} = \mu I(r,z).\tag{2}$$

The laser parameters used in the simulation can be found in Table **I**; the total simulation time is 10 µs.

Before enamel ablation can be modelled, we need to define two sets of BCs, one for the thermal simulations and one for the stress simulations.

2.1 Boundary Conditions for stress analyses

Let us first consider the problem of determining the most appropriate BCs for the stress analyses. Periodic BCs are not appropriate to laser ablation modelling because in this case the material can only expand up. Making the nodes at the lateral and bottom surfaces of the model entirely fix is also not appropriate because it renders lateral expansion impossible. However, we expect that a modified version of this second method will lead to more appropriate BCs.

4

The modification consists of surrounding a small enamel model (named model <u>Small</u>) with a layer of another material (named *Restrain-layer*), which makes the transition between the fixed nodes and the centre of the model. The Restrain-layer must have properties that allow the centre of the model to expand while accounting for the constraining effect and expansion of the bulk.

In order to determine which values of the Restrain-layer properties are appropriate, it is necessary to compare the results obtained using model <u>Small</u> with a reference. Given the impossibility of comparing these results with experimental data (to the best of our knowledge, the necessary information is not available), the only possible way to assess the adequacy of the proposed BCs is resorting to modelling. Therefore, we decided to create a larger enamel model (named model <u>Large</u>) which would be the reference against which we would compare the results from model <u>Small</u>. Model <u>Large</u> (dimensions $65 * 65 * 20 \ \mu m^3$) represents a single piece of human dental enamel, in which the nodes of the lateral and bottom surfaces are fix. Despite the fact that dental enamel has a microstructure, we did not include it in any of the models considered in this paper. As a result, the elements in model <u>Large</u> are assigned the material properties of hydroxyapatite (the main component of dental enamel), with the exception of the absorption coefficient, which is relative to human dental enamel (see Table **II**). Model <u>Small</u> (dimensions $19 * 19 * 20 \ \mu m^3$) is more complex: it has a central region (the *Core* of the model) made of enamel, and an outer-layer made of a different material, the already mentioned Restrain-layer. The lateral and bottom nodes of model <u>Small</u> are also fix. Since models <u>Large</u> and <u>Small</u> have the same height, only a lateral Restrain-layer is considered for model <u>Small</u> (see Fig. 1). The Restrain-layer effectively provides the BCs for the Core of model <u>Small</u> so that, by adjusting the material properties of the Restrain-layer, the Core can effectively reproduce the dynamic temperature, displacement and stress fields at the centre of model <u>Large</u>.

The mechanical properties of the Restrain-layer must have values such that nodes in surface B experience the same stress and displacement as nodes in surface A (see Fig. 1). In order to estimate these values, we assumed that enamel (a brittle material) obeys a linear-elastic stress-strain relationship until it fractures. For a bar, this relationship is

$$\sigma = E \frac{\Delta \ell}{\ell} \tag{3}$$

where σ is the stress, E is the Young's modulus of the material, $\Delta \ell$ is the elongation suffered by the bar and ℓ is the initial length of the bar. The Restrain-layer also obeys this relationship, because there is no physical reason to use more complex material models for this layer.

By applying eq. 3 to models <u>Large</u> and <u>Small</u> (see Fig. 1), and considering that $\Delta \ell_{enamel(surface\ A)} = \Delta \ell_{Restrain-layer(surface\ B)}$ and $\sigma_{enamel(surface\ A)} = \sigma_{Restrain-layer(surface\ B)}$, we obtain an expression to estimate $E_{Restrain-layer}$:

$$E_{Restrain-layer} = E_{enamel} \frac{\ell_{Restrain-layer}}{\ell_{enamel}} \tag{4}$$

The Restrain-layer must also account for the thermal expansion which the region it replaces undergoes and its effect on the central part of the model. The thermal expansion coefficient, α, of a bar is given by

$$\alpha = \frac{\Delta \ell}{\ell} \frac{1}{\Delta T} \tag{5}$$

where ΔT is the change in temperature. By applying Eq. 5 to models <u>Large</u> and <u>Small</u>, and considering that $\Delta\ell_{enamel(surface\ A)} = \Delta\ell_{Restrain-layer(surface\ B)}$ and that $\Delta T_{enamel} = \Delta T_{Restrain-layer}$, we obtain an expression to estimate $\alpha_{Restrain-Layer}$:

$$\alpha_{\mathrm{Re}\,strain-layer} = \frac{\alpha_{enamel} \cdot \ell_{\,enamel}}{\ell_{\,\mathrm{Re}\,strain-layer}} \tag{6}$$

Only the thermal expansion coefficients along the X and Y directions ($\alpha_{Restrain-layer,xx}$ and $\alpha_{Restrain-layer,yy}$) are scaled according to Eq. 6 because no Restrain-layer is used at the bottom of model <u>Small</u>.

2.2 Boundary conditions for thermal analyses

Model <u>Large</u> represents a piece of material which is thermally insulated from its surroundings by the lateral and bottom surfaces; the top surface is in contact with the atmosphere, but heat losses by radiation and convection during 10 μs will be small. The temperature gradient and, consequently, the heat transfer along XY in models <u>Large</u> and <u>Small</u> will be negligible. For these reasons, both models <u>Small</u> and <u>Large</u> have adiabatic BCs during the thermal analysis.

2.2 Applying thermal and stress boundary conditions to the dental enamel model

Having developed a methodology for obtaining appropriate BCs for the stress and thermal analyses, we proceeded to apply them to an enamel model, named <u>Dental</u>, which represents a small piece of enamel *part of a human tooth* (dimensions 23 * 23 * 35 μm^3, 187765 elements) under CO_2 laser radiation. Our objective is to study the temporal evolution of the stress and displacement fields in this model.

Because the region of the tooth in which we are interested is surrounded by material in all directions except at the top, model <u>Dental</u> must have a *Lateral Restrain-layer,* with thickness $\ell_{\text{Lateral Restrain-layer}} = 2.8$ μm and a *Bottom Restrain-layer,* with thickness $\ell_{\text{Bottom Restrain-layer}} = 0.6$ μm, corresponding to the bottom layer of elements (images are not shown) .

To estimate $E_{\text{Lateral Restrain-layer}}$, we used eq. 4 and assumed that model <u>Dental</u> was laterally surrounded by 6 mm of enamel; $\alpha_{\text{Lateral Restrain-layer,xx}}$ and $\alpha_{\text{Lateral Restrain-layer,yy}}$ were estimated using Eq. 6 and assuming that the radius of the area undergoing expansion around our model was 0.2 mm, which corresponds to the laser beam radius (see Table **I**).

The bottom part of the model does not undergo any significant temperature rise during the simulation time, so $\alpha_{\text{Bottom Restrain-layer}}$ can be set to 0. When estimating $E_{\text{Bottom Restrain-layer}}$, we assumed that beneath the simulated region were 6 mm of dentine (E = 15 GPa).

In order to account for heat losses to the bulk of the tooth, the bottom layer of elements was given a large density during the thermal analysis, thus acting like a heat sink. All material properties are given in Table **II**.

3. Results and discussion

The temperature distribution at all instants during the simulated 10 μs is similar in all studied models. The maximum temperature reached (at the end of the laser pulse) is 160 ºC, at the top surface. Temperature decreases with depth. The only noticeable temperature gradients occur in direction OZ (see Fig. 2).

The equivalent Von Mises stress (VMS) fields obtained at the end of 10 μs in model <u>Large</u> and model <u>Small</u> are presented in Fig. 1. The VMS is a useful quantity to which resort when analysing results, because it combines the 9 components of the stress tensor at each element into a single scalar. Using the BCs described in section **2**, the areas at the centre of models <u>Large</u> and <u>Small</u> show similar VMS. The stress and displacement magnitude as a function of time for two elements and two nodes at the XY centre of both models is shown on

8

Fig. 3; one of the elements/nodes is located at the irradiated surface; the other is inside the model (see Fig. 1, regions A1, A2, B1, B2). The dynamic evolution of the stress and displacement values at the centre of model <u>Small</u> is qualitatively identical and quantitatively very similar to model <u>Large</u>. The displacement magnitude of all the nodes that were compared between both models differs less than 10 %. The difference in the VMS between both models is, in the regions of interest, less than 20%; this difference tends to increase with depth, which indicates that care must be used when interpreting results from regions deep inside the model, particularly from a quantitative perspective. The characteristic frequency of the displacement magnitude in model <u>Small</u> is 9.3 MHz, very close to the one in model <u>Large</u> (10.5 MHz). Natural frequency extraction analyses confirmed that these are the most important natural frequencies of vibration of both structures.

The results obtained with model <u>Small</u> indicate that the BCs applied to this model with appropriate Restrain-Layer properties allow it to replicate the results obtained with model <u>Large</u>, while remaining simple in conception and easy to apply to any model of the nature of those presented here, with linear material behaviour (such as illustrated in Eqs. 3 and 5).

Fig. 4 shows the VMS and the displacement magnitude as a function of time for two elements and two nodes at the XY centre of model <u>Dental</u>, one located at the free surface and the other located at a depth of 2.5 µm. The displacement graphs suggest that heating and consequent dilation of the material cause it to vibrate after the laser pulse, with a characteristic frequency of around 0.4 MHz, and with amplitudes comparable to the total average displacement that the nodes underwent. However, this does not seem to translate into a stress wave of equivalent frequency. Since the model does not include energy dissipation mechanisms, further work is necessary to ascertain the timescale in which this vibration will attenuate. The VMS at the element located inside the model rises steeply during the laser pulse, but afterwards remains approximately constant. The VMS at the surface element, on the other hand, reaches a maximum right after the end of the laser pulse, and afterwards

decreases, becoming lower than the stress at the middle element when t > 4 μs. This exponential decrease is much steeper than the exponential decrease of the temperature with time. These non-intuitive results are consequence of the complex 3D stress-state of the simulated structure, and suggest that FE models with discretization above the micrometer scale will not be able to capture the stress and displacement states that occur at this scale. Further models with similar BCs and accounting for the mesostructure of the material will be developed to assess the implications of local stress and displacements such as those reported here to the ablation mechanisms.

4. Conclusions

In this work we addressed the important issue of developing and testing a new approach to apply BCs for micrometer-scale FE ablation models of brittle materials by mid-IR lasers. Our results indicate that these BCs represent an accurate and yet simple way of simulating the response of a small piece of material which is a part of a larger object to laser irradiation, without the need to simulate the response of the entire larger object, and still accurately capturing the dynamics of the displacement and stress fields in the material.

Applying these BCs to a continuous model of human dental enamel under CO_2 pulsed radiation allowed us to study the dynamic displacement and stress fields generated inside the material during and after one laser pulse, and to obtain simulation results which are not intuitively obvious. These results suggest that the highest values of stress occur at the surface, at the end of the laser pulse, but they decrease rapidly to significantly lower values than those found at the depth of just a few microns inside the material. Also, even though the laser pulse duration is too long to allow stress confinement effects, the laser still induces a vibration in the material.

Since most ceramic materials have mesoscopic structure, it is of significant importance to apply the proposed BCs to dynamic models of ablation by mid-IR lasers of such brittle

10

materials which include this mesostructure, in order to assess its role during ablation. These currently inexistent models will help to further understand the ablation mechanisms in ceramic materials as well as to optimize existing experimental procedures.

References

1. M. Stoneham, M.M.D. Ramos and R.M. Ribeiro, Appl. Phys. A, 69 (1999) s81.

2. A.M. Stoneham and J.H. Harding, Nat. Mater., 2 (2003) 77.

3. B. Majaron, P. Plestenjak and M. Lukac, Appl. Phys. B, 69 (2003) 71.

4. L.V. Zhigilei, P.B.S. Kodali and B.J. Garrison, J. Phys. Chem. B, 101 (1997) 2028.

5. A. Vila Verde, M.M.D. Ramos, R.M. Ribeiro and M. Stoneham, in P. Rechmann, D. Fried and T. Hennig (Eds), Proceedings of SPIE, Vol. 4950, SPIE, 2003, p.72.

6. A. Vila Verde, M.M.D. Ramos, R.M. Ribeiro and A.M. Stoneham, Thin Sol. Films, 453-454 (2003) 89.

7. H.M. Niemz, Laser-Tissue Interactions - Fundamentals and applications, Springer-Verlag, Berlin, 1st ed.,1996.

8. M.J. Zuerlein, D. Fried, J.D.B. Featherstone and W. Seka, IEEE J. Sel. Top. Quantum Electron., 5 (1999) 1083.

9. H.H. Moroi, K. Okimoto, R. Moroi and Y. Terada, Int. J. Prosthodontics, 6 (1993) 564, in 'Dental Tables' at http://www.lib.umich.edu/.

10. M. Braden, in Y. Kawamura (Ed), Physiology of Oral Tissues, Frontiers of Oral Physiology, Vol 2, S. Karger AG, Basel, 1976, p.21.

11. D.E. Grenoble, K.J. L, K.L. Dunn, R.S. Gilmore and K.L. Murty, J. Biomed. Mater. Res., 6 (1972) 221, in 'Dental Tables' at http://www.lib.umich.edu/.

12. J. Czernuszka, in D. Bloor, M.C. Flemings, R. Brook, S. Mahajan and R. Cahn (Eds), The encyclopedia of advanced materials, Vol 4, Elsevier Science Ltd, Cambridge, Great Britain, 1994, p. 1076.

Table I: Laser parameters. Notice that I_0 is below the ablation threshold of enamel.

Type of laser	CO_2 (10.6 μm)
Pulse duration (μs)	0.35
Maximum absorbed intensity, I_0 (J.m^{-2}.s^{-1})	1.2×10^{10}
Number of pulses	1
Laser beam radius (mm)	0.2

Table II: Material properties

	Enamel	Model Small Restrain-layer	Model Dental Lateral Restrain-layer	Bottom Restrain-layer
Absorption coefficient (cm^{-1})	825 [8]	825	825	825
Density ($kg.m^{-3}$)	3.1×10^3	3.1×10^3	3.1×10^3	Therm. anal.: 3.1×10^6 Stress anal.: 3.1×10^3
Thermal conductivity ($J.s^{-1}.m^{-1}.°C^{-1}$)	1.3 [9]	1.3	1.3	1.3
Specific heat ($J.kg^{-1}.°C^{-1}$)	880 [9]	880	880	880
Young's modulus ($N.m^{-2}$)	1.1×10^{11} [10]	1.0×10^{10}	5×10^7	1.5×10^6
Poisson's ratio	0.28 [11]	0.28	0.28	0.28
Expansion coefficient ($°C^{-1}$)	1.6×10^{-5} [12]	$\alpha_{xx} = 1.8 \times 10^{-4}$ $\alpha_{yy} = 1.8 \times 10^{-4}$ $\alpha_{zz} = 1.6 \times 10^{-5}$	$\alpha_{xx} = 1 \times 10^{-3}$ $\alpha_{yy} = 1 \times 10^{-3}$ $\alpha_{zz} = 1.6 \times 10^{-5}$	0

Fig. 1 – Von Mises stress (N/cm^2) for a) model <u>Large</u> (204323 nodes, 192296 elements) and

b) model <u>Small</u> (21141 nodes, 18928 elements), for t = 10 µs. Regions A1, A2, B1 and B2

identify the location of the elements and nodes mentioned in Fig. 3. Only half the model is

shown in each image.

Fig. 2 – Temperature distribution for model Large, at the end of the laser pulse (t = 0.35 µs).

Fig. 3 – Von Mises stress and displacement magnitude as a function of time for elements and

nodes (shown in Fig. 1) located at the XY centre of models <u>Large</u> and <u>Small</u>.

Fig. 4 - Von Mises stress and displacement magnitude as a function of time for two

elements/nodes at the XY centre of model <u>Dental</u>, located at the free surface and at a depth of
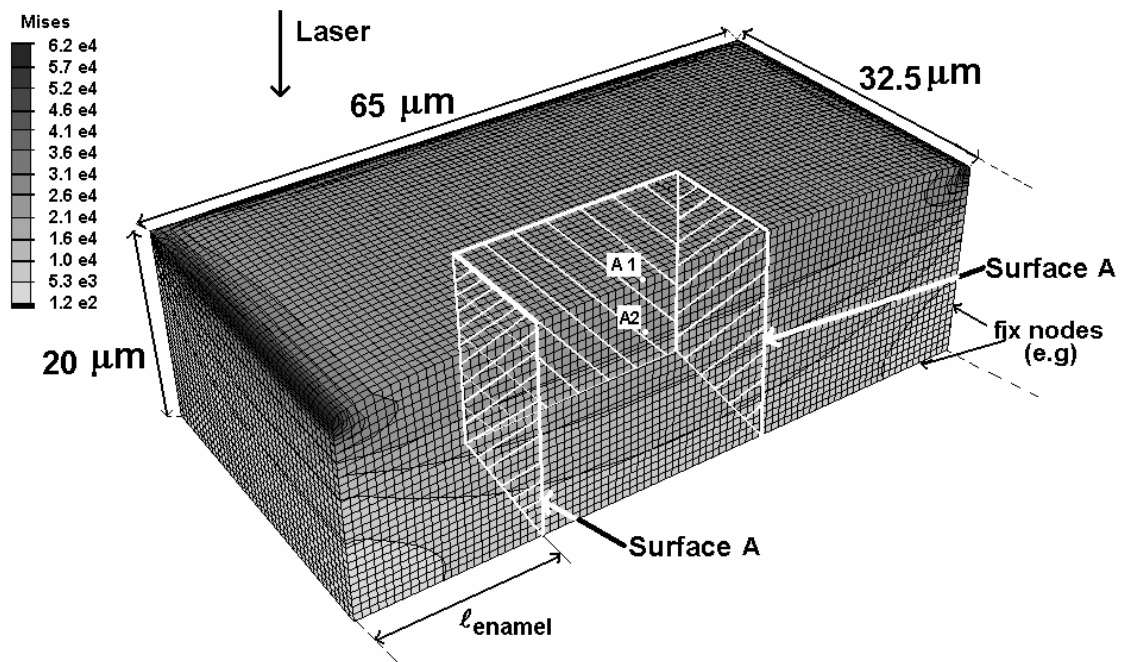
2.5 µm.

figure 1a
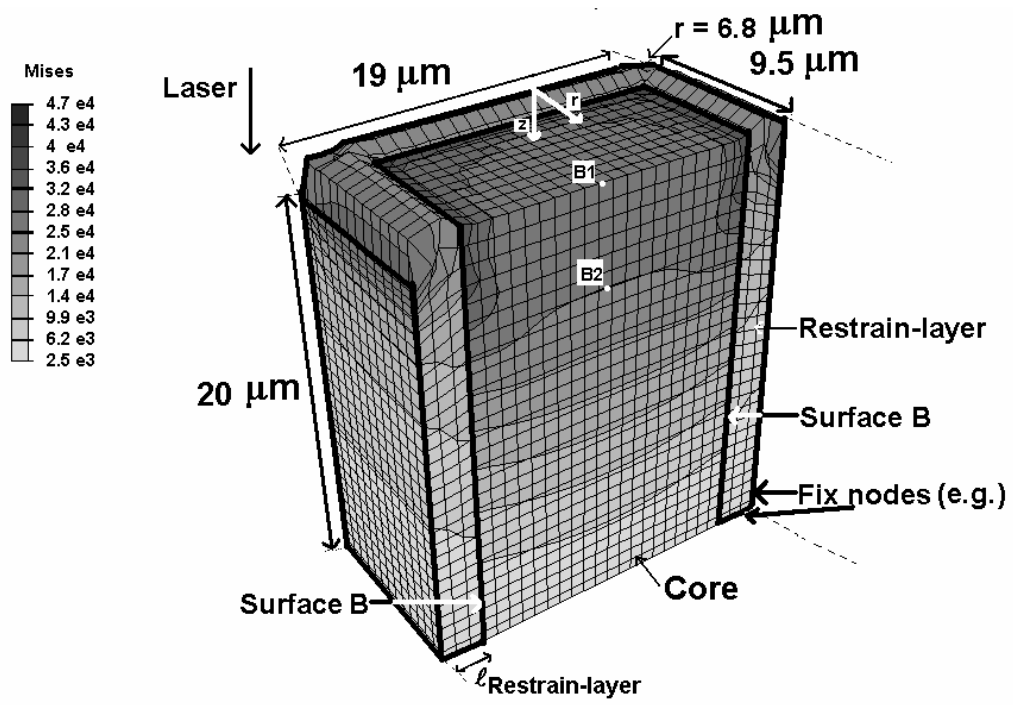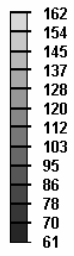
figure 1b

figure 2

Model "Large"   Von Mises stress   Model "Small"
                          (N/cm²)

Surface Element   35000   Surface Element
(Region A1)   30000   (Region B1)
                  25000
Middle Element   20000   Middle Element
(Region A2)   15000   (Region B2)
                  10000
                   5000
                      0

Time (μs)   Time (μs)

Displacement magnitude
                    (nm)

Surface Node   35   Surface Node
(Region A1)   30   (Region B1)
                    25
                    20
Middle Node   15   Middle Node
(Region A2)   10   (Region B2)
                     5
                     0

Time (μs)   Time (μs)

fffigure 3

figure 4